The H_2O maser flare region in the Orion-KL nebula

L. I. Matveenko

Institute for Space Research, USSR Academy of Sciences, Moscow

D. A. Graham

Max-Planck-Institut für Radioastronomie, Bonn

P. J. Diamond

National Radio Astronomy Observatory, Charlottesville, Virginia

(Submitted August 19, 1988)

Pis'ma Astron. Zh. **14**, 1101–1122 (December 1988)

VLBI studies of the fine structure in the Orion-KL water-maser flare region during 1979–1987 show that most of the radio emission comes from a chain of compact sources oriented along PA$\approx -80°$. Each source is ≤ 0.1 AU in diameter and has a brightness temperature $T_b \sim 10^{17}$ K. The width of the individual line-profile components is $\Delta f \leq 7$ kHz. There is a velocity gradient of 0.41 km sec^{-1} AU^{-1} along the chain. The compact features are linearly polarized by $p \geq 80\%$, and the polarization angle exhibits a 9°.2/AU gradient. The H_2O molecules have column and volume densities of $\sim 10^{18}$ cm^{-2}, 10^4 cm^{-3}. The masers are not saturated; their kinetic temperature $T_k \leq 120$ K. Evidently the infrared pump is anisotropic. The outburst region might be a family of expanding protoplanetary rings of 6 AU radius, spreading apart at 3.8 km/sec and rotating at 5 km/sec about a 0.7 $M_\odot$ protostar.

1. INTRODUCTION

The active processes of star and planetary-system formation that operate in many interstellar complexes of gas and dust are accompanied by powerful maser radio emission. A unique sign of this activity, not yet fully understood, is the intense maser flaring that may occur in the water vapor radio line: one component of the line profile will suddenly strengthen and remain at a high level for a long time. What mechanism triggers these outbursts and how they might relate to the process of protoplanetary ring formation are questions of great importance.

Maser outbursts are so rare as to be hard to investigate. The first strong flare of this kind was observed[1] on 6 June 1971 in the object W49. Within about 5 min the radio flux density of the component at V = −1.8 km/sec jumped by more than an order of magnitude, reaching F ~ 10^5 Jy. Subsequent measurements with the Simeiz–Haystack radio interferometer showed that the flare emission zone measured just 1-2 AU across, so that its brightness temperature reached $T_b \gtrsim 10^{16}$ K. So extreme a T_b value suggests that the radiation was beamed; the anisotropy might derive from the source geometry, or else the radiation may be coherent.

A second instance was encountered in the Orion Nebula in 1979. Between September 4 (F = $7 \cdot 10^4$ Jy) and September 24 (F = $5 \cdot 10^5$ Jy) the emission of the V ≈ 8 km/sec component started to brighten,[2,3] reaching $2 \cdot 10^6$ Jy no later than October 15. Several intervals of intense masing were later observed in this region. As Fig. 1 demonstrates,[4] the radiation peaked toward the end of 1979, in mid-1980, in later 1983, and in early 1984. The shortest outburst, late in 1983, lasted less than 2^d. The highest flux density attained was F ~ $8 \cdot 10^6$ Jy.

Position measurements of the survey region during 1977-1979, prior to the high activity, disclosed no evidence of motion in the plane of the sky.[5] Nor has there been any appreciable change in the radial component of the flare-zone velocity. VLBI studies of the spatial structure of that zone during 1979-1987 (at the epochs marked in Fig. 1) have revealed an intricate, well-organized pattern in the distribution of the component maser sources. The outcome of these studies is set forth below.

2. FINE STRUCTURE OF FLARE REGION

VLBI measurements were first acquired on 1979 September 24, during the initial stage of the outburst in the Kleinmann–Low nebula, at which time F = $0.5 \cdot 10^6$ Jy; observations have been made on a number of subsequent occasions. Table I gives the site of each interferometer station, the antenna diameter, the dates when the Orion-KL source was observed with the telescopes indicated by crosses, and the corresponding flux densities of the maser flare.

Figure 2 charts the coverage of the (u, v) plane for one of the most comprehensive experiments, in which radio telescopes from both the European

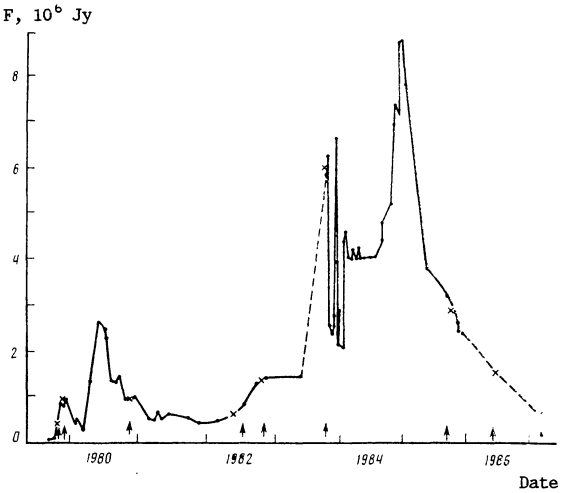

FIG. 1. Evolution of the radio flux density F during the H_2O maser flares in the Orion-KL nebula.[4] Arrows mark the epochs of VLBI observations; crosses designate the corresponding flux-density measurements.

 0360-0327/88/06 0468-10 03.00

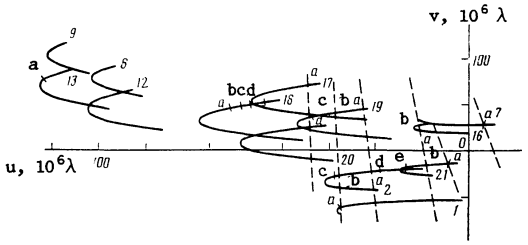

FIG. 2. Coverage of the (u, v) plane for selected pairings of the first seven VLBI stations listed in Table I: 1) Cr–On; 2) Cr–Ef; 3) Cr–Hs; 4) Cr–GB; 5) Cr–VLA; 6) Cr–OV; 7) On–Ef; 8) On–Hs; 9) On–GB; 10) On–VLA; 11) On–OV; 12) Ef–Hs; 13) Ef–GB; 14) Ef–VLA; 15) Ef–OV; 16) Hs–GB; 17) Hs–VLA; 18) Hs–OV; 19) GB–VLA; 20) GB–OV; 21) VLA–OV. The points marked along the visibility curves are identified in Sec. 3 and in the legend of Fig. 4.

and the American VLBI networks participated. The angular resolution (the fringe spacing) ranged from 0".040 for the shortest baseline (OV–VLA) to 0".0003 for the longest (OV–Cr). This extensive sample of baselines has enabled us to remove the ambiguities involved in finding the distances between the compact components, and to determine their relative positions.

As a rule the flare H_2O line had a simple Gaussian profile distorted to some extent by a time-variable asymmetry.

In radio interferometry the profile of a line may undergo significant changes, implying that the emission region has a complex spatial structure, with comparatively narrow lines originating in separate compact regions. To illustrate, Fig. 3 shows some line profiles computed for a double source that emits equal-intensity lines having Gaussian profiles $P(f) = Ae^{-Bf^2}$. The two components are assumed to have a relative velocity equivalent to $0.8\Delta f$, where Δf is the linewidth (FWHM).

The combined line profile of two such point sources is given by the vector sum $\bar{P}_0(f) = \Sigma \bar{P}_i(f_i)$. (the amplitudes of the component vectors depend on frequency, while the "relative phase" $\phi = \pi \cdot \Delta\theta/\phi_{fr}$ measures the angular distance $\Delta\theta$ separating the component sources in units of the fringe width ϕ_{fr}): $P_0(f) = \sqrt{P_1^2 + P_2^2 + 2P_1P_2\cos\varphi}$. The $\bar{P}_0(f)$ signal will have a phase $\psi_0(f) = \sin^{-1}\left[\frac{P_i(f)}{P_0(f)}\sin\varphi\right]$.

In Fig. 3 each panel plots the frequency dependence of the phase $\psi_0(f)$ and amplitude $P_0(f)$ (the line profile) for model sources whose two components are separated by different distances, that is, for differing angular resolutions. If the separation equals the fringe width ($\Delta\theta = \phi_{fr}$, $\phi = 180°$), the phase $\psi_0(f)$ exhibits a 180° jump, and the corresponding line profile develops a central dip to zero. If the source components have a substantial angular size, comparable with the fringe width, then smoothing takes place within the source regions, evening out the observed profiles and phase curves. In the case of different-intensity components (Fig. 3b) the profile peaks differ in height, but the deep central dip and the 180° phase jump (when $\Delta\theta = \phi_{fr}$) persist.

An emission region comprising several pointlike components will have a more intricate line profile, depending on the angular resolution, but the number of peaks in the profile will match the number of components.

When we turn to the VLBI data for Orion-KL we find that the flare line profiles display features

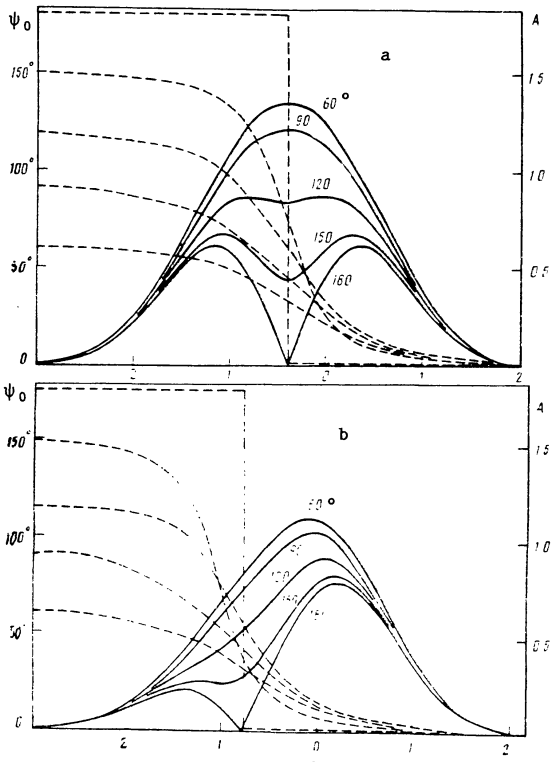

FIG. 3. Theoretical curves for the frequency dependence of the correlated flux (solid curves, representing radio-line profiles of a maser flare) and phase (dashed) of the signal from a two-component source, for five relative angular resolutions ϕ. a) Equal-intensity components, $P_1 = P_2$; b) $P_1 = 0.5P_2$.

TABLE I. VLBI Observations of H_2O Maser in Orion-KL

Radio telescope site	Aperture m	1979 23.IX	1979 16.XI	1982 1.XII	1983 10.XI	1984 6.II	1985 2.X	1986 26.V	1987 16.II
Simeiz, Crimea (Cr)	22	×	×	×	×	×	×	×	×
Effelsberg, W. G. (Ef)	100		×	×	×	×	×	×	×
Onsala, Sweden (Os)	20		×	×	×	×	×	×	×
Haystack Obs., Mass.	37		×			×	×		
Green Bank, W. Va (GB)	43		×			×	×		
Socorro, N.M. (VLA)	25						×		
Owens Valley, Calif. (OV)	40						×		
Pushchino, Moscow	22	×							
Flux density	F, 10^6 Jy	0.5	1.7	1.0	5.0	3.2	0.6	2.1	0.5
Profile width	Δf, kHz	30	32.6	37	48	52	42	28	26

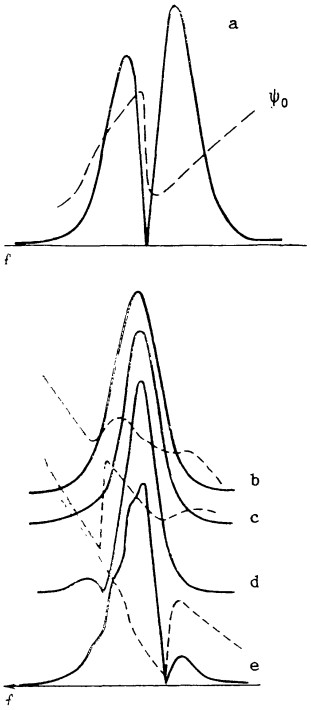

FIG. 4. Orion-KL correlated-flux profiles (solid curves) and phases (dashed), observed with differing baselines at different hour angles. a) On–Ef, 20^h (on 1 December 1982; Fig. 2, curve 7, point b); b, c, d) Cr–Ef (1 December 1982) at 20^h12^m, 20^h55^m, 22^h53^m (Fig. 2, curve 2, pints c, d, e, respectively); e) Cr–Ef, 4^h57^m (10 November 1983; Fig. 2, curve 2, point a).

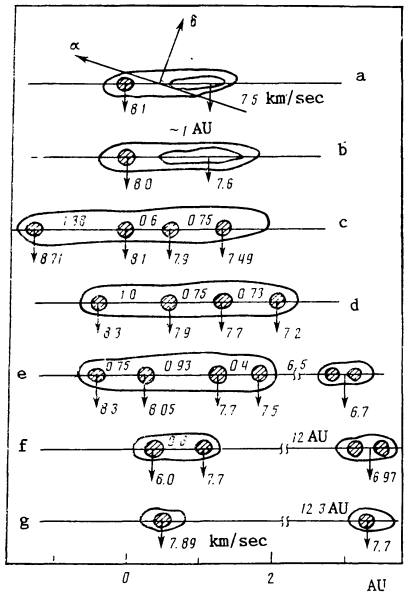

FIG. 5. The distribution of compact structures in the H_2O maser flare region on: a) 25 Sep 1979; b) 16 Nov 1979; c) 1 Dec 1982; d) 10 Oct 1985; e) 2 Oct 1985; f) 26 May 1986; g) 16 Feb 1987.

resembling these model curves. As Fig. 4 demonstrates, the observational curves indeed depend on the angular resolution, that is, on the baseline and hour angle. The profiles are doubled, with accompanying side features, and the phases do show jumps as great as 180°.

3. RESULTS OF OBSERVATIONS

1. The first interferometry of the maser flare region during its initial development was performed with the Cr–Pu baseline on 25 September 1979 ($F = 0.5\cdot10^6$ Jy). The H_2O line profile was approximately 30 kHz wide and had a high-frequency tail. It was found that the outburst site had a compound structure, with an extended (2.5 AU diameter) and a compact (0.25 AU) component (see Fig. 5a) having $T_b \approx 3\cdot10^{14}$ and $5\cdot10^{15}$ K, respectively.

Most of the emission emanated from the compact region, whose radial velocity $V \approx 8.1$ km/sec; for the extended component, $V \approx 7.5$ km/sec, accounting for the higher-frequency radiation. The compact region was shown[2] to consist of "point" sources whose spatial and velocity distribution suggested an analogy to protoplanetary rings.

2. VLBI measurements in November 1979 confirmed the existence of the compact region and indicated that it was located ~1 AU away from the extended source (Fig. 5b). These observations were made with the Cr–Ef and GB–Hs interferometers. The outburst had meanwhile brightened to $F = 1.7\cdot10^6$ Jy as T_b in the compact region increased[6] to $5\cdot10^{16}$ K; the profile width was 32.6 kHz.

3. In December 1982 measurements were made with the VLBI triad Cr–Ef–On and provided a more detailed map of the flare structure. The flux density reached $1\cdot10^6$ Jy, and the H_2O line broadened to $\Delta f = 37$ kHz. Major changes in the maser configuration had occurred over the previous 3 yr (Fig. 5c), as is clearly apparent from the Cr–Ef (Fig. 4, curves b-d; $\phi_{fr} \approx 0''.0015$) and Cr–On line profiles; yet the profile for the short On–Ef baseline (Fig. 4a; $\phi_{fr} \approx 0''.005$) was not affected. Evidently, then, the overall size of the masing region was at most $0''.005$ or 2.5 AU.

For the longer baselines the line profile acquires a deep dip in certain position angles of the projected baseline, suggesting the presence of compact emission components separated by a distance comparable with the fringe width. At such times the interference-signal phase also may jump by 180° (Figs. 4b-e).

Four principal compact structures can be identified in the emission region, arrayed in position angle $PA \approx -80°$ (Fig. 5c). Successive pairs are separated by $\Delta L = 1.38$, 0.6, 0.75 AU; the components have velocities of 8.7, 8.1, 7.9, 7.5 km/sec, respectively. Each is at most 0.2 AU in diameter, so the brightness temperatures $T_b \gtrsim 10^{17}$ K. The profiles of the lines emitted by the individual compact sources are ~10 kHz wide. The velocities show a uniform gradient $\Delta V/\Delta L \approx 0.4$ km·sec^{-1}·AU^{-1} along the array.

Polarimetry was carried out at each station: in left- and right-circular polarization of Simeiz (alternating every $0^h.5$), in linear polarization of Effelsberg, and in left-circular at Onsala. Analysis indicates that the compact soruces are >80% linearly polarized, since the Simeiz left- and right-circular signals correlate practically identically with the left-circular polarization at Onsala. Analysis indicates that the compact sources are >80% linearly polarized, since the Simeiz left- and right-circular signals correlate practically identically with the left-circular polarization of Onsala.

4. On 10 October 1983 another series of VLBI observations was begun and they recorded a new

phase of maser activity (Fig. 1). The peak intensity was $F \approx 5 \cdot 10^6$ Jy, the profile width $\Delta f = 48$ kHz. During this active phase the high-frequency part of the line profile was enhanced (see Figs. 7a, b below). The Cr–Ef measurements confirm the four-component structure (Fig. 5d). Curves e in Fig. 4 show the line profile and phase variation at an epoch corresponding to point a on curve 2 in Fig. 2. The four components again are arrayed in PA $\approx -80°$; they are separated by 1.0, 0.75, 0.73 AU, respectively, and their velocities are 8.3, 7.9, 7.7, 7.2 km/sec.

In late October, 15-kHz resolution polarimetry was carried out with the RT-22 at Simeiz,[24] and the position angle χ of the polarization plane was found to vary within the line profile by $d\chi/df = 0°.5/\text{kHz}$. At the line center $\chi = -16°$. The percentage polarization was p = 70% in mid-profile, rising slightly to 72% in the high-frequency part.[7,8]

Measurements on 13 December 1983 confirmed the strengthening of the high-frequency wing in the profile (Fig. 7a) and showed a more complex χ-variation. The changes in χ correlate directly with those in the line profile, being determined by variations of the separate components; hence the radiation of each component has its own χ-value. Thus $\chi \approx -13°, -20°, -40°$ for the low-f, center, and high-f components, respectively. The high-f component (V = 7.2 km/sec) dominates the observed variability: it was an order of magnitude brighter in October 1983 than in 1982. In December its flux rose further, causing the measured change in χ. The profile width was 43.5 kHz.

In February 1984 the high-f wing was again enhanced (Fig. 7c), and the profile had broadened to 52 kHz. Although χ varies markedly across the profile, the values themselves are about the same as in December: $\chi \approx -15°, -20°, -40°$ for the low-f, center, and high-f components, respectively. The high-f component (V = 7.2 km/sec) dominates the observed variability: it was an order of magnitude brighter in October 1983 than in 1982. In December its flux rose further, causing the measured change in χ. The profile width was 43.5 kHz.

In February 1984 the high-f wing was again enhanced (Fig. 7c), and the profile had broadened to 52 kHz. Although χ varies markedly across the profile, the values themselves are about the same as in December: $\chi \approx -15°, -22°$ in the low-f wing and mid-profile, respectively In the high-f wing χ reaches $-43°$, but p is lower than before, dropping to 65%. Comparison between December 1983 and February 1984 suggests that the component sources maintained steady χ-values.

5. On 3-5 October 1985 a comprehensive survey of the flare region was conducted with the global VLBI network. Seven radio telescopes participated (Table I), achieving the optimum angular resolution feasible with ground-based antennas. The (u, v) visibility curves for this experiment are plotted in Fig. 2. On this occasion F reached $0.6 \cdot 10^6$ Jy, and the profile width was 42 kHz (as before, the profile was measured with 15-kHz resolution; the line-width measurement includes a Gaussian correction for the filter transmission band).

As Fig. 7d demonstrates, the contribution of the high-frequency tail has much diminished.

The 1985 experiment provides the best information on how the behavior of the profile depends on the baseline length and orientation relative to the survey region (see Figs. 2 and 6). The dashed lines in Fig. 2 join points corresponding to identical line profile and phase variations. These dashed lines have slopes representing similar projections along position angles $\xi \approx -73°, -85°$ for the short and long baselines, respectively, implying that the compact bright structures are distributed along a smooth arc.

For the shortest baselines (points 7a and 21a in Figs. 2 and 6) an interesting peculiarity develops: the line profile splits, with a new low-frequency component appearing at V = 6.7 km/sec, separated from the main group by 6.5 AU (Fig. 5e). It is less than 1 AU across. The four bright, compact sites making up the main group are separated by 1.5, 1.85, 0.8 AU and have velocities of 8.3, 8.05, 7.7, 7.5 km/sec. The longest-baseline data indicate that the component angular sizes are $\lesssim 0.1$ AU. Perhaps along with these four bright components, others may exist which have weakened but which coincide with features observed earlier.

At the end of Fig. 6 is a long-baseline profile for point a on curve 13 of Fig. 2. Probably the compact regions are embedded in halos or are superimposed on an extended maser-emission background.

The polarization of the main group reaches 70% (Fig. 7d), with the plane of polarization at $\chi \approx -16°$. For the low velocity component $p \leq 60\%$ and $\chi = -22°$. The changes in the low-f profile with respect to hour angle indicate a complex structure for this part of the emission region; perhaps it comprises a pair of compact sources separated by ~1 AU (Fig. 5e).

6. In May 1986 the line profile experienced a major modification: it began to bifurcate, showing a contour similar to the August 15 profile illustrated in Fig. 7e. The principal (V = 7.8 km/sec) component has strengthened, peaking at $F = 2.1 \cdot 10^6$ Jy, with $\Delta f = 28$ kHz, A lower-velocity source, shifted by 0.7 km/sec, occupies a band $\Delta f = 33.8$ kHz and reaches $F \approx 0.51 F_{max} \approx 1 \cdot 10^6$ Jy. These two components, according to the Cr–Ef–On data, are separated by ~12 AU (Fig. 5f). They measure about 0.5, 0.5 AU across, and have $T_b \approx 8 \cdot 10^{17}, 4 \cdot 10^{17}$ K.

The compact higher-velocity regin probably has two subcomponents ~0.6 AU apart. The low-velocity compact region is surrounded by an extended (~7.5 AU) component having V = 6.97 km/sec, displaced ~1.5 AU from the emission peak. This compact region similarly may have a compound structure, comprising several "point" sources.

Polarimetry on August 15 (Fig. 7e) shows a linear polarization reaching p = 70% in the new (6.97 km/sec) region, with $\chi = -30°$. In the main (7.86 km/sec) component, $p \approx 60\%$ and $\chi = -18°$.

7. Finally, on 16 February 1987, during a period of waning activity, the line profile remained double (Fig. 7f). The principal (7.89 km/sec) component had $F = 0.5 \cdot 10^6$ Jy, while the low-velocity (7.2 km/sec) component peaked at $0.14 \cdot 10^6$ Jy. The emission bandwidths remained about the same as before: $\Delta f = 26$ kHz. The separation between the two components was 12.3 AU (Fig. 5g). As for the polarization, p maintained a level of (60-70)% for both components, but there was a significant difference in χ ($-12°, -28°$, respectively).

4. DISCUSSION

Figure 5 is indicative of the complex structure of the H_2O maser flare region in Orion-KL. Several

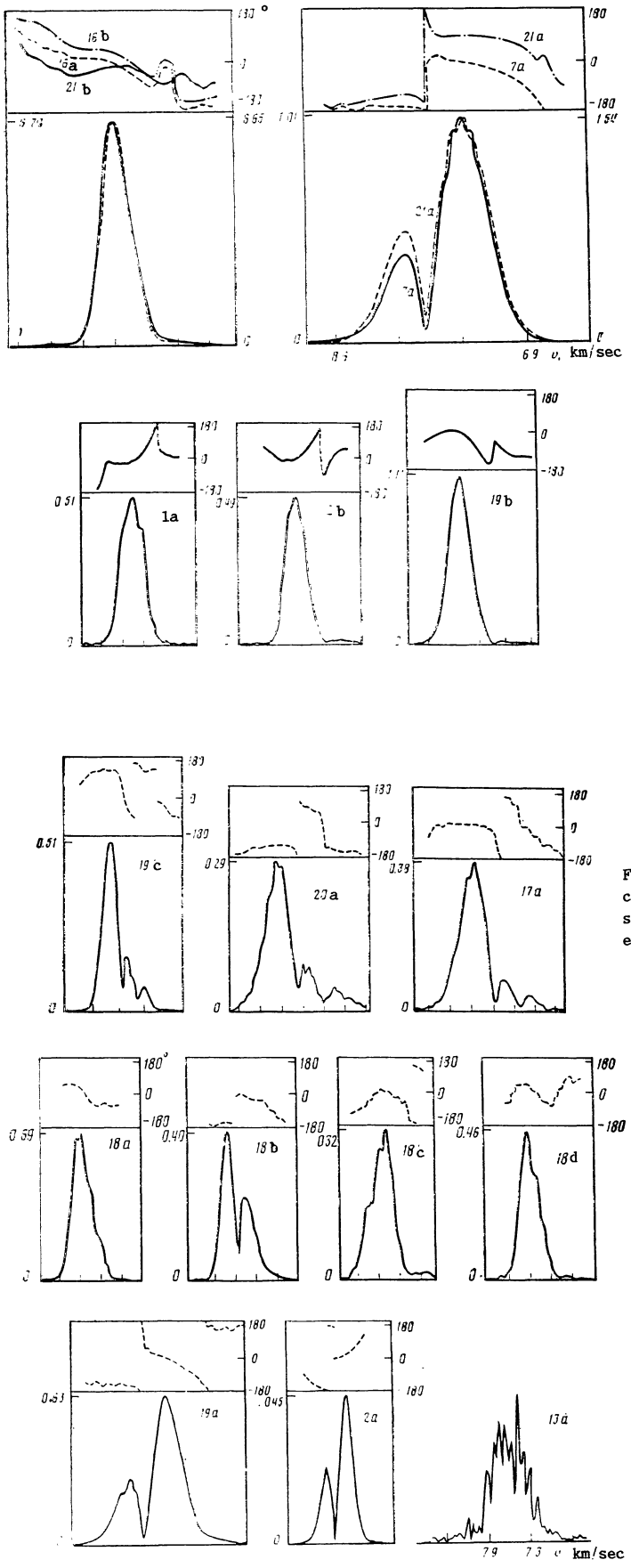

FIG. 6. Correlated-flux line profiles (iower pannels) and phase curves recorded by various VLBI antenna pairs at epochs corresponding to the points marked along the curves in Fig. 2. In each case the velocity axis is divided into intervals of 0.6 km/sec.

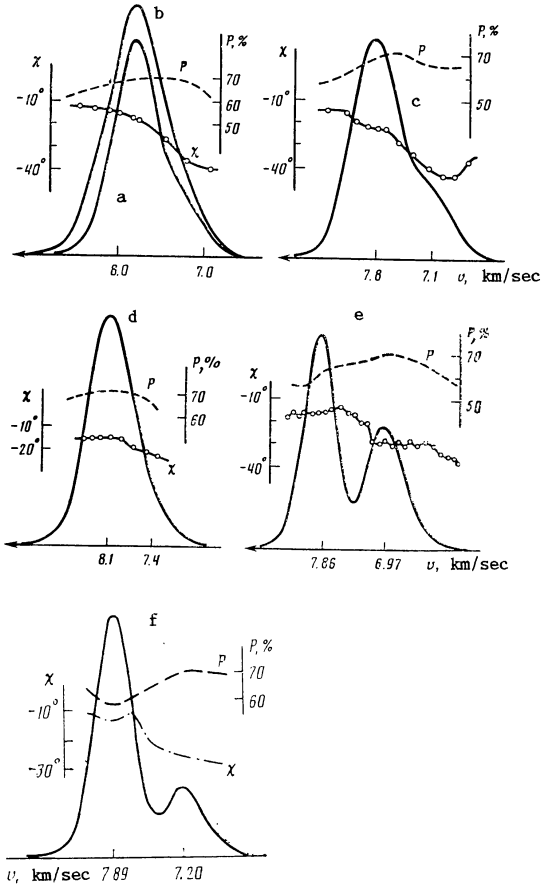

FIG. 7. H_2O maser line profiles and the corresponding trends of the percentage polarization p and its position angle χ across the profile, as observed on: a) 13 Dec 1983; b) 23 Nov 1983 (same units); c) 6 Feb, 1984; d) 2 Oct, 1985; e) 15 Aug, 1986; f) 16 Feb 1987.

bright, compact features are present, forming a chain oriented along a position angle that varies from ξ = −73° to −85°, depending on whether the VLBI baseline is short or long. Each component is ~0.1 AU in diameter, and their separations range from 0.4 to 1.4 AU. The positions of the individual components are accurate to ~0.01 AU.

Usually two to four bright compact sites are observed, clustering within a ~2.5 AU region. They have radial velocities of 7.2-8.7 km/sec, measured to approximately 0.1 km/sec accuracy. The velocities of the components vary insignificantly, by amounts within the errors, and may perhaps be constant.

On the other hand the emission of the components is quite variable, although the variations of the separate components seem to be uncorrelated. Each compact feature emits a narrow spectral line: the Gaussian fit is at most 10 kHz wide. Consequently the uncorrelated fluctuations in the radiation of the individual components, which moreover have different longitudinal velocity components, induce changes in the flare line profile: the width varies and asymmetry develops, with the profile sometimes acquiring a high-velocity tail.

The positions of the components definitely correlate with their velocities (Fig. 8, solid curve). If the motion were Keplerian we would have $R \propto V^{-2}$; indeed, as Fig. 9 demonstrates, the experimental data conform to a linear law, with a velocity gradient $\Delta V/\Delta L = 0.41 \pm 0.05$ km·sec^{-1}·AU^{-1}. If this observed gradient is maintained throughout the emission zone of each component, then the line of a component measuring $\ell_c \approx 0.1$ AU across would be broadened by $(\Delta V/\Delta L)\cdot\ell_c = 0.041 \pm 0.005$ km/sec. Thus the broadening of the observed lines amounts to $\lesssim 3$ kHz, and the emission line of a "stationary" source should have an intrinsic width $\Delta f_c < 7$ kHz.

From our value for the velocity gradient we can estimate the length of the chain directly, using the width of the line profile recorded by a single antenna. The narrowest profiles (Δf = 22-27 kHz) would correspond to component spaced about 0.8-1.0 AU apart.

The maser flare radiation is polarized by up to (60-70)%. The polarization angle χ varies over the line profile, and also undergoes substantial variations with time (Fig. 7). These fluctuations are complicated, and reflect the changing relative contribution of the separate radio components.

The middle of the line profile (within the 15-kHz filter passband) is formed by the radiation of several neighboring components; the vector sum of their contributions gives the composite polarized radiation and its angle χ. The profile wings are dominated by a single outlying component, so in those parts of the profile the χ-value is closer to the inherent value for each component. For the low-velocity (V < 7 km/sec) components, $\chi \approx -15°$, while the high-velocity ones (v > 8 km/sec) have $\chi \approx -15°$. The dashed line in Fig. 8 indicates how the limiting χ-values depend on velocity. On the average the plane of polarization rotates by $\Delta\chi/\Delta V = 20°\cdot(\text{km/sec})^{-1}$, or, if we introduce the velocity dependence of the components' relative position, by $\Delta\chi/\Delta L = 9°.2/\text{AU}$.

The components' differences in χ have hardly any effect on the total amount of polarized radiation received in the 15-kHz passband; hence the measured amplitude p (Fig. 7) reflects the true p-variations across the line profile. On the high-frequency side p reaches ~70%, diminishing to 60% on the low-f side. For the individual compact sources, according to the VLBI data,[9,10] p > 80%. Since a variety of depolarization effects (including background and instrumental factors) will weaken the polarized com-

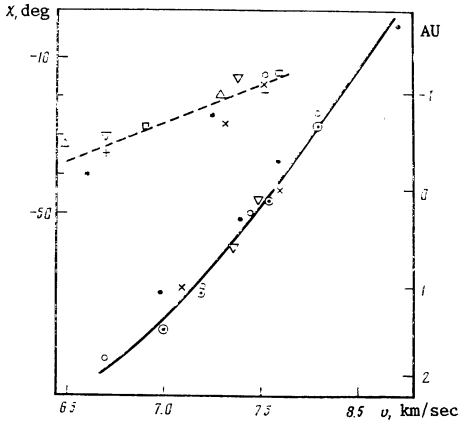

FIG. 8. Mutual displacement ΔL of the component sources (solid curve, right-hand scale) and position angle χ of the plane of polarization (dashed curve, left-hand scale) as functions of the measured velocity.

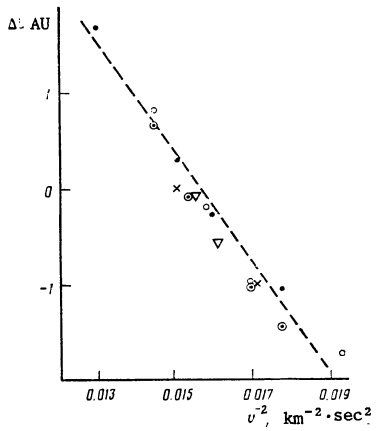

FIG. 9. Mutual displacement ΔL of the components as a function of V^{-2}.

ponent, the actual maser flare emission — the radiation from the individual compact sources — is evidently almost completely linearly polarized.

In 1983-1984 the flare line profile began to exhibit some low-velocity radiation (Fig. 7), probably associated with the V ≈ 7.2 km/sec component. By 1985 the flare region had developed a structural component 6.5 AU away (Fig. 5e), with V = 6.7 km/sec and a flux density of 10^5 Jy, about 15% of the peak value. In 1986 the profile split into two well-defined parts (Fig. 7f) corresponding to regions separated by ~12 AU; the low-velocity component acquired a speed of 6.97 km/sec, with F = $7 \cdot 10^5$ Jy. The separation increased slightly (to ΔL = 12.3 AU) in 1987. Again the profile resolves into two parts (Fig. 7g), but the low-V peak (F ≃ $1.5 \cdot 10^5$ Jy) has dropped to the ~30% level. The split may result from either a spatial displacement between the components or a narrowing of the line profile for each separate source. The main part of the observed profile has a width ≲ 26-28 kHz. In the low-velocity region the polarization parameters p = (66-70)%, χ = −(30°-40°).

Figure 10 illustrates how the separation of the two components and the radial velocity of the low-V source have evolved with time. The longitudinal velocity component has been changing at a rate of ~0.45 km·sec^{-1}·yr^{-1}, and the velocity in the plane of the sky is ~40.3 km/sec. The line profile of the low-V source is 34 kHz wide.

We find, then, that the H_2O maser flare region in Orion-KL has the following properties:

1. It is a highly organized structure, with a chain of about four compact components being confined to a ~2.5 AU interval, supplemented by a source ~10 AU away from the chain.

2. The compact components are ~0.1 AU in diameter.

3. In the plane of the sky the chain is oriented along PA ξ = −(73°-85°).

4. The components have a longitudinal velocity component of ≈ 8 km/sec.

5. Their velocities correlate with their separation from each other: the velocity gradient ΔV/ΔL = 0.41 km·sec^{-1}·AU^{-1}.

6. The compact sources emit narrow (Δf ≲ 7 kHz) spectral lines.

7. Their radiation is variable.

8. No correlation is discernible in the radio variability of contiguous components.

9. The compact sources contribute at most 30% of the peak flare intensity.

10. At maximum the maser outburst produced a flux density F ≲ $8 \cdot 10^6$ Jy.

11. The radio emission of the compact sources is almost totally polarized (p ≳ 80%).

12. In the low-frequency part of the line profile the polarization is enhanced.

13. The orientation of the plane of polarization varies across the line profile, with an angle gradient Δχ/ΔL = 9°.2/AU.

14. By the close of the present observations a subsidiary H_2O maser source was located about 10 AU away from the main region and was moving in the plane of the sky at a projected velocity V ≈ 40.3 km/sec. The longitudinal velocity was changing by 0.45 km·sec^{-1}·yr^{-1}. The radiation was linearly polarized by p = (60-70)%, with the plane of polarization oriented in position angle χ = −(30°-40°). The radio flux density was F = 10^5 Jy, and the H_2O line width was ~34 kHz.

5. INTERPRETATION OF RESULTS

It has been established[6,11,12] that the H_2O maser flare site (α = 5h32m46s.6, δ = −5°24'28".7) lies 1".2 ± 1" west of the Orion-KL nucleus and coincides with an expanding, rotating shell around a massive (10-30 $M_\odot$) star. The shell is 2" or 10^3 AU in radius and is expanding at 2.1 km/sec. The star itself is traveling relative to the Local Standard of Rest[13] at V_{LSR} ≈ 5.5 km/sec. Nearby is the powerful infrared source IRC 4, which probably is serving to pump the flare maser emission. The λ ≈ 20 μ flux has been holding nearly constant during the course of the outburst.[5]

The hot Orion-KL core[14] has a radial velocity V_{LSR} ≈ 5 km/sec, temperature T = 700 K, and total luminosity L = 10^5 $L_\odot$; it dominates the volume luminosity of the whole region. Surrounding the core is a disk of radius R ≈ 1 AU, oriented in PA ≈ 60°. The disk temperature T_K = 60-100 K. Judging from the orientation of grains in this region, the magnetic field runs parallel to the disk.

In some cases the individual compact sources have a flux density F ≈ 10^6 Jy, which, in view of their ~0".0002 angular size, is equivalent to a brightness temperature T_b ≳ 10^{17} K. If the emission were isotropic, such a source would have a 10^3 $L_\odot$ luminosity in the H_2O line, in excess of the power observed for the infrared pump. The maser outburst also has a T_b value well above the limit set by the Stark effect, suggesting, as does the luminosity, that the radiation is highly directional (solid angle Ω ≲ 10^{-4} sr)

Either of two factors may account for this strong beaming: coherence, or a purely geometric effect (such as the emission of an end-on filament). Water vapor molecules could not be confined to a filamentary configuration by a magnetic field. Filaments might however, be formed by gravitational forces in the circumstellar disk, and be part of a ring. In that event the chain of component sources could represent protoplanetary rings whose plane is facing the observer (Fig. 11). In tangential directions we would view these "filaments" endwise. The filament length ℓ will be determined by the apparent size of the

source ($d \lesssim 0.2$ AU) and the directivity of the radiation: $\ell \approx d \cdot \Omega^{-0.5} \approx 20$ AU.

But the apparent size is dictated not by the physical diameter of the sources in the plane of the sky but by the optical-depth differential. In the unsaturated-maser case, the corresponding change in intensity will amount to $I/I_0 = e^{-\Delta\tau}$. If we measure the apparent angular size by an e-fold drop in I, the equivalent differential will be $\Delta\tau = 1$. In a homogeneous ring, τ will be determined by the geometrical path length: $\tau \sim \ell$.

For an unsaturated maser the total optical depth of a source can be established from its T_b value, the background temperature T_{bk}, and the contribution T_s from spontaneous emission: $\tau \approx \ln [T_b/(T_{bk} + T_s)]$. In the case of Orion-KL, $T_{bk} + T_s \lesssim 100°K$; accordingly $\tau \approx 35$. If instead the maser is partially saturated, then τ should be even larger, and the apparent angular size will more closely represent the physical size. Thus the flare source acquires its apparent angular size within a region where τ drops to a level of a few percent, at a "cusp" in the optical depth (Fig. 11).

The τ differential will depend on the relative thickness d/x of the ring:

$$\frac{\tau}{\tau_{max}} \simeq \sqrt{\frac{x}{d}} - \left(1 - \frac{d}{R}\right)\sqrt{\frac{x}{d} - 1}, \qquad (1)$$

where the coordinate x is measured from the outer edge of the ring toward its center (Fig. 11). The thickness should probably not exceed the separation between the compact sources: $d \leq 0.5$ AU.

In a thin ring the apparent size of a component source will be insensitive to its radius R; it will be determined mainly by the first term in the expression (1), that is, by the ring thickness d. In our case $\tau \approx 35$, $d = 0.5$ AU, and in relative units the compact source will have an apparent angular size $\ell_k \approx (d - x)/d \approx 2\Delta x/\tau_{max}$, equivalent to ~0.03 AU if $\Delta\tau = 1$. The size of the compact region will be somewhat larger in the perpendicular direction, so that the source should have an elongated shape. Actually the apparent size should depend strongly on how the water vapor molecules are distributed over the ring cross section. Thus a compact source ~0.1 AU across might acquire its apparent size through the masing of a ring source with a ~0.5 AU cross section.

As shown above, the emission of the compact region is highly beamed. In the case of a ring, the directivity is given by $\Omega \approx (0.1d/\ell)^2$, so that in Orion-KL we should have $\ell \geq 5$ AU. Hence the ring radius should be $R \geq 0.01d/8\Omega \approx 6$ AU.

On the other hand, we can estimate R from the relation $\Delta V/\Delta R = V/2R$. The observations give $\Delta V/\Delta L = 0.41$ km·sec^{-1}·AU^{-1} and the central star has $V_{LSR} = 5.5$ km/sec, so the projected rotational velocity of the rings is $V_{rot\parallel} \approx 2.6$ km/sec. Corrected for projection, $V_{rot} = V_{rot\parallel}/\cos\theta \approx 2.9$ km/sec (the velocity of the source is determined by the velocity of the region at the maser input). Thus the maser flare region will be defined by a ring of radius $R = (V/2)\Delta R/\Delta V \approx 3.5$ AU, a value smaller than found in the preceding estimate.

This disparity could be explained if the ring were expanding. The ring's rotational radial velocity is $V_{rot\parallel} = 2.9$ km/sec, directed away from the observer (Fig. 11), but the radial component $V_{exp\parallel}$ of the expansion velocity would be approaching the observer. The measured velocity V = 2.9 km/sec would represent the difference $V_{rot\parallel}$. If we take R = 6 AU, then the upper limit on the rotational velocity set by Keplerian motion would be $V_{rot} = 5$ km/sec, or $V_{rot\parallel} = 4.5$ km/sec projected onto the line of sight. The projected component of the ring expansion velocity will be $V_{exp\parallel} = 1.6$ km/sec, so that the ring would actually be expanding at $V_{exp} = 3.8$ km/sec. Thus the radio flare region would form a ring that concurrently is expanding at 3.8 km/sec and rotating at 5 km/sec. The radius of this ring (or family of rings) would be $R \approx 6$ AU, and the central star should therefore have a mass $M = V^2R/G = 0.16\ M_\odot$ in the expanding-ring case.

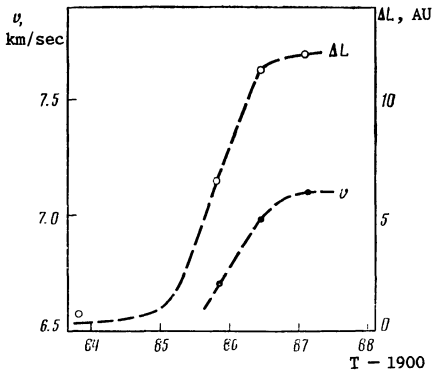

FIG. 10. Evolution of the line-of-sight velocity and displacement of the low-frequency component of Orion-KL.

The correlation observed between the relative placement and squared velocity of the components is practically linear (Fig. 9), with a slope $\alpha = GM$ 570 AU·km^2/sec^2. Hence we obtain a direct mass estimate $M = \alpha/G = 1.33 \cdot 10^{33}$ g $= 0.7\ M_\odot$ for the central star.

A ring structure for the maser would explain in a natural manner why the compact sources — individual rotating rings — appear to remain stationary. Although the rings would in fact be expanding at $V_{exp} = 3.8$ km/sec, their corresponding change in radius would amount to ≈ 0.7 AU/yr or 0".0014/yr, and their mutual displacement would be effectively unmeasurable.

Temperature of rings. The line width Δf_r [kHz] is directly related to the kinetic temperature T_k [in kelvins] of the radiating material: $\Delta f_r = 3.73 T_k^{\frac{1}{2}}$. If the maser is unsaturated, its optical depth will determine the apparent width Δf of the line: $\Delta f = \Delta f_r \tau^{-\frac{1}{2}}$. Accordingly $T_k = (3.73)^{-2}\Delta f^2 \tau$.

For the compact components $\tau \approx 35$ and $\Delta f \approx 7$ kHz. In that case the water vapor molecules would have $T_k \approx 120$ K, close to the 60-100 K value derived from the CO and NH_3 lines.[14] This is nearly the optimum temperature at which protoplanetary rings can develop from a mixture of dust and ice.[15]

The low T_k value calls for radiative pumping. Although the pump source might be the powerful infrared emitter IRC 4 nearby, collisional pumping by hot electrons[16] also is possible, of course, but it would then be harder to explain why the maser radiation is so highly polarized.

Since the 20-μ flux from IRC 4 has shown little change,[5] one might expect the level of H_2O emission

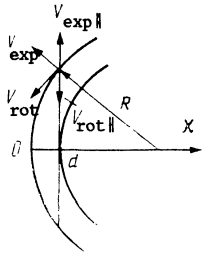

FIG. 11. A protoplanetary ring of radius R and thickness d. The observer is at the top of the diagram.

from the flare region to remain steady. But if one assumes the flaring to be caused by an unsaturated maser, the radio variability observed could result from quite small (~10%) changes in τ. Such effects might be produced by fluctuations in, say, the amount of dust screening the pump or the water vapor content.

Water molecule density. The optical depth of a maser source is given by $\tau = kn_{exc}\ell$, where k is a constant for any given transition and n_{exc} denotes the number density of excited molecules. For $\tau = 35$ we should have[17,18] $n_{exc}\ell \lesssim 10^{16}$ cm^{-2}. In our case $\ell = 5$ AU, so $n_{exc} \lesssim 10^2$ cm^{-3}. At T_k 100 K the fraction of water vapor molecules in the signal K-levels might be ~10^{-2}; the total density of H_2O molecules in the flare region would then be $n \sim 10^4$ cm^{-3}. The values we have obtained for τ and the corresponding molecular column density suggest that the maser might be partially saturated (Ref. 17).

A ring viewed edgewise will emit a double line profile whose two components correspond to the tangential directions. In our case only one component of the profile is observed — perhaps because of pumping peculiarities, or else the H_2O molecules may be distributed nonuniformly over the ring. In particular, a portion of the ring might be shielded by dust and not receive enough pump radiation.

Polarization. The compact H_2O maser flare sites display a remarkably strong linear polarization ($p \gtrsim 80\%$) whose position angle χ varies with the separation between the source components at a rate of 8°.2/AU or 20°·(km/sec)$^{-1}$.

One well-known mechanism for linearly polarizing the radiation of a maser is normal Zeeman splitting, with strong interaction and a saturated regime.[19,20] Being a paramagnetic substance, water vapor requires unusually high magnetic field strengths[14] for Zeeman splitting to occur, roughly 1 gauss/kHz; splitting comparable to the radio-line width would call for a ~50 gauss field. Moreover in our case the extreme apparent T_b of the maser components and the variability of their radiation are hard to reconcile with a saturated regime.

These conflicts, however, can be resolved quite satisfactorily by a beamed-pump model. The linear polarization of maser emission comes about because of an alignment of particle spins.[19] In astrophysical contexts we generally encounter nonequilibrium systems in which the spins are oriented by a directive flux of particles or infrared radiation (spin tuning). Radiation passing through such a medium will become linearly polarized. If a magnetic field is present it will control the orientation of the plane of polarization. This subject has been investigated by Western and Watson,[21,22] who have shown that a maser with anisotropic pumping can achieve 100% polarization, and in an unsaturated regime. The magnetic field will scarcely affect the polarization amplitude — only its orientation.

In our case the pump is stellar infrared radiation, and it will be highly beamed with respect to the rings. The angle subtended at the maser input will be of order 10^{-3} sr. Thus the emission of the unsaturated ring-maser ought to be almost 100% linearly polarized. The situation here corresponds to Western and Watson's case c, the tangential emission of a ring.[22]

In Orion, masing is also observed in the SiO lines.[23] The profile is double and suggests the emission of an edgewise disk. As in our case the SiO radiation is linearly polarized, although considerably more weakly, and χ rotates by ~50° within each profile feature. The SiO data have been modeled[23] by a rotating, expanding disk whose magnetic field is parallel to the velocity vector at each point. The polarization vector would be parallel to the magnetic field vector, varying in orientation in different parts of the disk.

Thanks to the high angular resolution of the VLBI experiment we have been able to resolve the "disk" into several concentric rings, which are rotating and expanding at $V_{rot} = 5$, $V_{exp} = 3.8$ km/sec. The rings revolve approximately once every 30 yr. A magnetic field might be frozen into the rings and control the orientation of the polarized radio emission.

Abraham et al.[4] interpret the variability in the intensity and the polarization amplitude p and position angle χ of the H_2O maser flare as the beamed radiation of a saturated maser processing along with the magnetic field within a small angle, with about a 4.2 yr period. In our model the nonuniform ring (or rings) will exhibit a similar effect; however, it will be caused not by precession but by rotation of the ring. The lack of any definite correlation between p and the radio intensity (whatever the flux density, p remains practically unchanged) is quite natural, because the polarization is induced by the beaming of the pump radiation. The p, χ variations observed at times of low activity may be attributed to the substrate — the changing contribution from the extended unpolarized background region.

6. CONCLUSIONS

The powerful H_2O maser radio emission observed in the Orion-KL nebula since 1979 represents the directional radiation of a family of concentric rings. Their radius $R \approx 6$ AU and thickness $d \approx 0.5$ AU. The rings are rotating at $V_{rot} \approx 5$ km/sec and expanding (spreading apart) at $V_{exp} \approx 3.8$ km/sec. We are viewing the radiation in the ring plane.

Water molecules are distributed nonuniformly over the rings, with a peak density $n_{H_2O} \sim 10^4$ cm^{-3} and a total column density $n_{H_2O}\ell \sim 10^{18}$ cm^{-2}. The H_2O molecules have a kinetic temperature $T_k \approx 120$ K. The maser is being pumped by the infrared radiation of a ~0.7 $M_\odot$ central star, or by the nearby infrared source IRC 4. It is masing in an unsaturate or only partially saturated regime. The maser amplification comes about as radiation emerges from a region of enhanced H_2O abundance in the tangential part of the ring. The dense part of the ~6 AU radius ring spends about 5 yr in the tangential position, determining the duration of the active phases. The short-term variability observed may be attributed